

## 2.B Electro-Optic Imaging of Surface Electric Fields in High-Power Photoconductive Switches

Semiconductor photoconductive switches have become increasingly useful for pulsed-power applications where high voltages must be switched on a short time scale. They are used in a variety of devices, including microwave generation, Pockel's cell drivers, and an innovative accelerator design.<sup>1,2</sup> There has been considerable interest in the design and operation of photoconductive switches, and various semiconductors have been investigated for use as switches, the most popular materials being silicon and GaAs. GaAs is particularly suited for high-voltage switches as its high resistivity ( $\rho > 10^7$  cm) makes it less susceptible to thermal runaway than other, less-resistive materials. This is very important, as the electric field between electrodes on a semiconductor photoconductive switch can be significant, with typical field strengths between 1 and 50 kV/cm. At these field strengths, switches will preferentially break down along the surface between electrodes. Surface breakdown is the primary failure mode for photoconductive switches and places a limit on their operation. The problem is compounded by the need to shorten the electrode gap to increase switching speed, thus increasing the electric field across the switch for a given bias voltage. Engineering considerations, such as the need to improve switch reliability, and the desire to explain certain physical phenomena associated with high-voltage switching have motivated the investigation of the dynamics of photoconductivity. Despite their relevance to switch engineering, the mechanisms of surface breakdown and photoconductivity are not well understood.

To better understand the physics of photoconductivity it is necessary to monitor a photoconductive switch during the switching process. Conventional analog or sampling oscilloscopes do not have the bandwidth to temporally resolve switch rise times of the order of a picosecond. However, greatly improved temporal resolution can be provided by sampling the switched output electro-optically. In this technique the birefringence of an electro-optic crystal, placed in the vicinity of an electronic circuit, is modified by stray electric fields surrounding the circuit. This electric field can then be measured by probing the electro-optic crystal with a fast, polarized optical pulse and monitoring the change in polarization. The duration of the optical pulse determines the bandwidth of the system, with an effective limit of about 1 THz due to crystal absorption. This technique has been used to measure the picosecond and subpicosecond output of electronic devices.<sup>3,4</sup>

Conventional electro-optic sampling techniques involve coupling the switched voltage output of a photoconductive switch to a strip line and measuring the voltage on the strip line electro-optically, remote from the switch. Such a measurement of the output waveform yields information

about the temporal evolution of the voltage at the output electrode of the switch but no information about the evolution of the electric field within the electrode gap itself. The electric field in the contact gap must be changing rapidly in both time and space as the gap is driven conductively by the optical-excitation pulse. By combining electro-optic sampling, short-pulse lasers, and imaging technology, an ultrafast, two-dimensional electro-optic imaging system has been developed that can monitor rapid variations of the electric field over an extended region in detail. This system can produce maps of the surface electric field between contacts on photoconductive switches that can be used to determine the electric-field configuration for different contact shapes, separation, and preparation.

This article details the development of the electro-optic imaging system and its application to the study of photoconductive switching, particularly in GaAs. The surface field between the electrodes on a GaAs photoconductive switch was monitored during switch operation; the collapse of the electric field was observed for various bias voltages and excitation conditions.

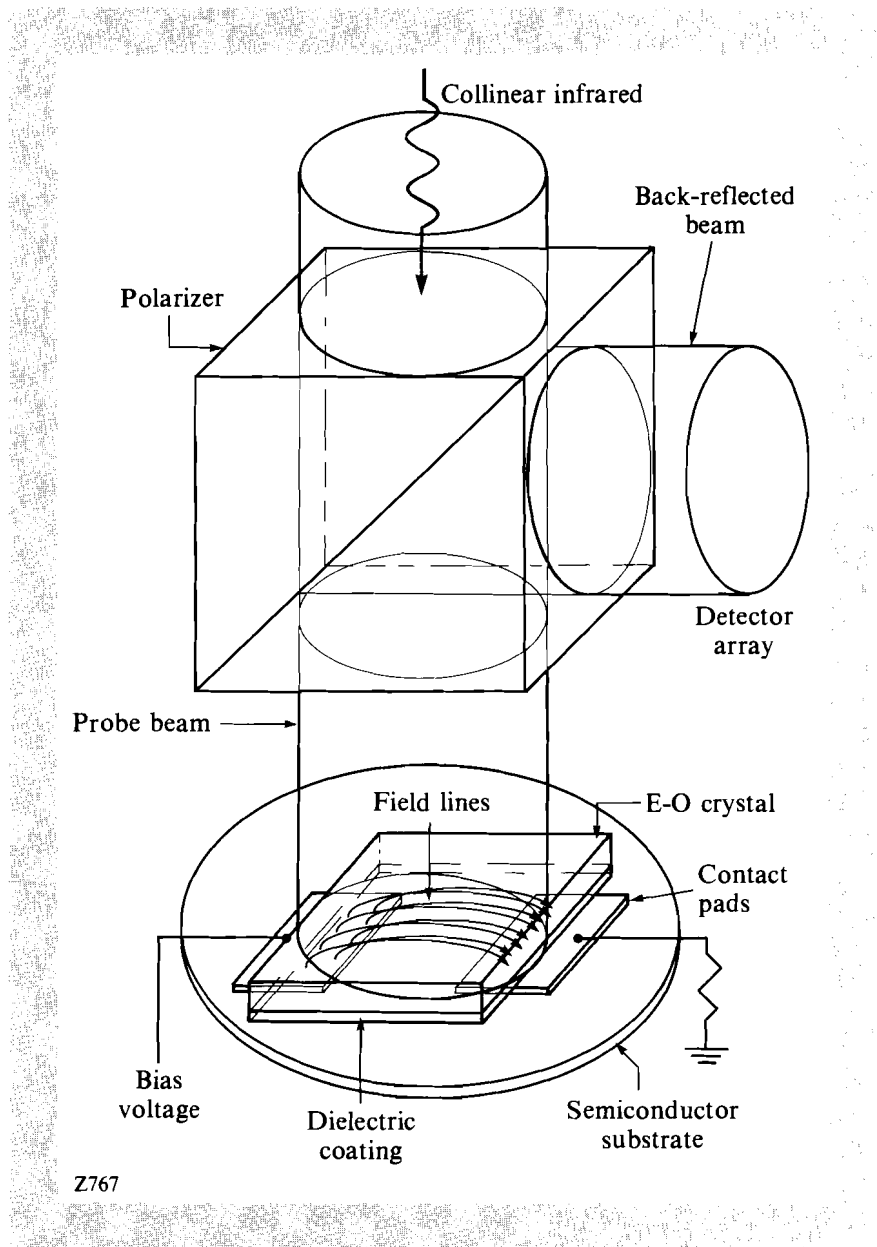
### System

The electro-optic imaging system represents the latest development in a series of optical probes utilizing the electro-optic effect to characterize surface electric fields between electrodes on semiconductor devices.<sup>5</sup> Earlier work involved the use of single-point or one-dimensional, time-averaged, electro-optic sampling. Extension of this work has produced the current two-dimensional, time-resolved, electro-optic imaging system, which can obtain full surface field maps in real time with picosecond temporal resolution.<sup>6,7</sup> This electro-optic probe is particularly suited for the study of high-field devices because the optical probe does not require any electrical connection to the device under test. Optical detection of the electric field is carried out using the electro-optic, or Pockel's, effect in which the birefringence of certain crystals can be altered by an electric field applied across the crystal. If a beam of polarized light traverses the crystal, the electrically induced birefringence will rotate the probe beam's polarization. This rotation can be detected and used to measure the electric field present in the crystal. The electric field in the crystal is not, necessarily, spatially uniform. If the probe beam only illuminates a small portion of the crystal, the electric field in that region only will be measured. A full measurement of the electric field would then require translation of the sampling point across the crystal. However, if the entire crystal is illuminated by the probe beam, the electric field at every point in the crystal will be interrogated. The probe beam will then be imprinted with an optical analog of the spatial electric-field distribution in the crystal. This is the essential operating principle of the two-dimensional electro-optic probe. Temporal resolution is obtained by using a pulsed laser as the probe beam. In effect, a snapshot of the instantaneous electric field is taken. To produce the desired effect, the crystal axis, optical polarization, and electric field must all be properly aligned.

Details of the probe beam, electrodes, and crystal geometry for the surface-field probe are shown in Figs. 42.23 and 42.24 for two different types

of photoconductive switches. Figure 42.23 shows the surface-field probe set up to measure the field of a photoconductive switch of a surface device type, i.e., the metallic contacts are in the same plane on the surface of a semiconductor substrate. Figure 42.24 shows the probe set up to measure the field of a bulk photoconductive switch, which has contacts on opposite faces of a rectangular slab of semiconductor. For either type of switch, the probe operation is the same; only the IR pump geometry is different. When a bias voltage is applied to the metallic contacts, an electric field is established between them with a fringing field extending above the surface of the semiconductor. The electro-optic crystal is placed directly on top of the switch, covering the contact gap completely. A dielectric mirror is bonded to the underside of the crystal. This reflection-coated side is in contact with

Fig. 42.23  
Detail of electro-optic probe set up to measure electric field above photoconductive switch of surface device type.



Z767

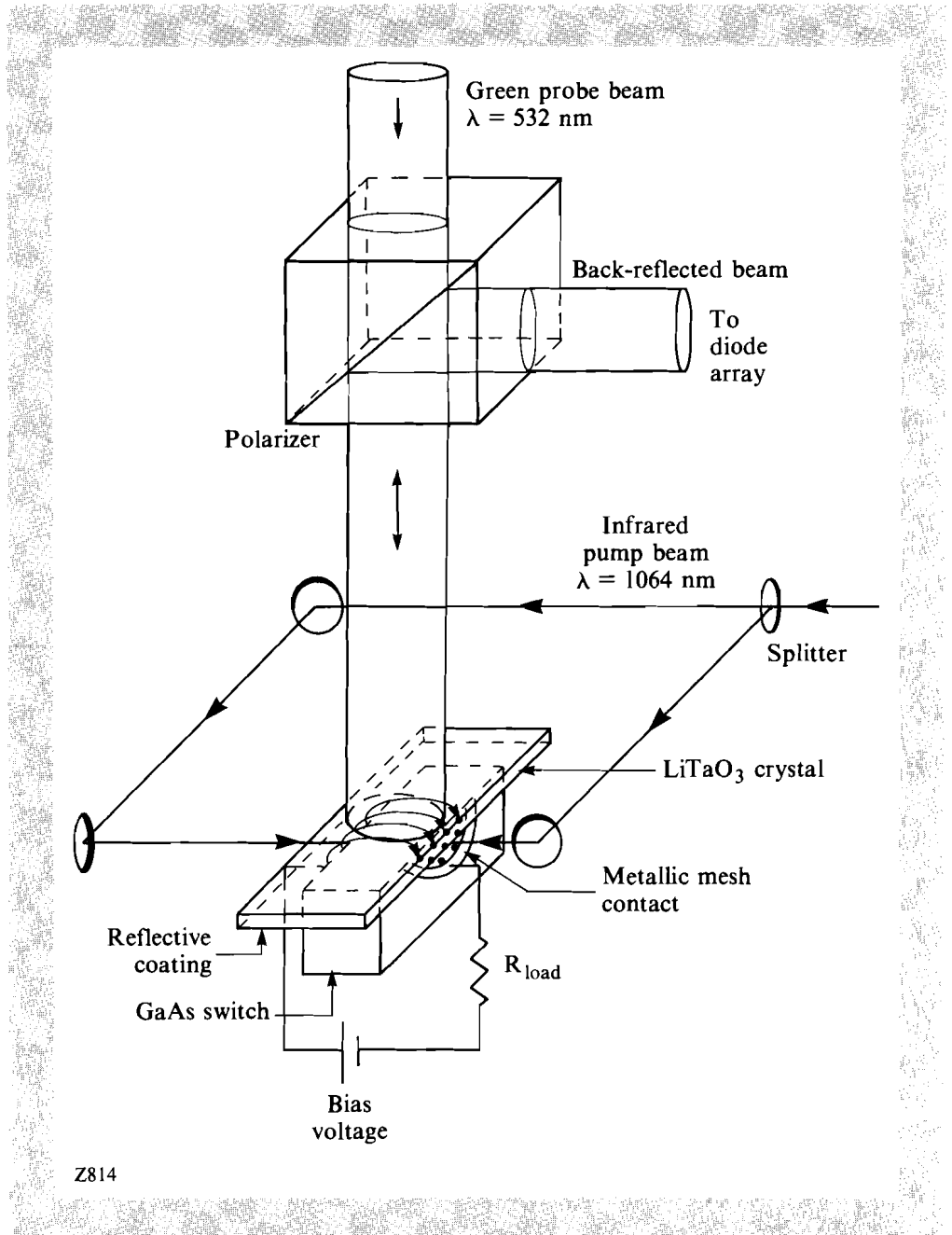


Fig. 42.24

Detail of electro-optic probe set up to measure electric field of GaAs bulk photoconductive switch.

the semiconductor. Therefore, the crystal is immersed in the fringing electric field of the contacts and its birefringence is altered by this surface field. The optical probe, visible green light with  $\lambda = 532 \text{ nm}$ , is polarized and directed onto the crystal and test switch. The probe-beam diameter is greater than the contact gap so that the entire contact gap is illuminated. The beam traverses

the crystal and is reflected back onto itself by the dielectric mirror on the semiconductor side of the crystal. The back-reflected beam, whose intensity is an optical analog of the electrically induced birefringence in the crystal, is imaged onto a two-dimensional diode array that records the intensity profile of the beam.

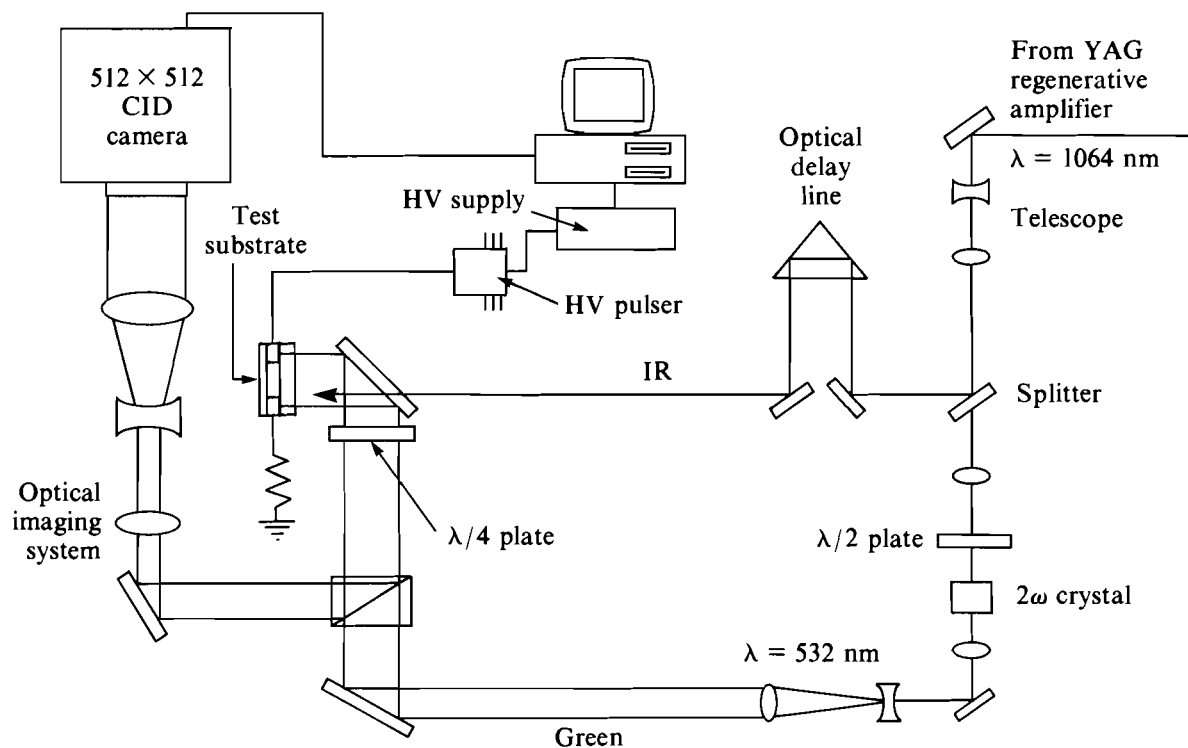
Each pixel in the array image has a corresponding point in the crystal. As the optical probe makes a double pass through the polarizer, the crystal can be considered to be between two crossed polarizers. The intensity at any given point in the cross section of the back-reflected beam will depend on the sine squared of the polarization rotation experienced by that particular beam element as it traversed the crystal. The transmission to a detector element  $(i, j)$  can be written as

$$T_{i,j}(V) = I_{i,j}(V) / I'_{i,j} = \sin^2[(\alpha_{i,j}E_{i,j} + \beta_{i,j})], \quad (1)$$

where  $I_{i,j}(V)$  is the light intensity measured at camera pixel  $(i, j)$  when a voltage  $V$  is applied to the electrodes;  $I'_{i,j}$  is the intensity that appears at the camera if 100% of the light is imaged onto the camera without bias voltage applied;  $E_{i,j}$  is the magnitude of the local electric field;  $\alpha_{i,j}$  is a constant for a given point  $(i, j)$  that relates the electro-optic coefficient<sup>8</sup> to the local electric field and whose value depends on material parameters, optical path length in the crystal, electrode geometry, and frequency of applied optical field; and  $\beta_{i,j}$  is a constant optical rotation due to static birefringence in the crystal and quarter-wave plate. To obtain the best response to the applied electric field, a quarter-wave plate is placed between the polarizer and crystal to optically bias the probe beam on the sine-squared transmission curve given by Eq. (1). By comparing the intensity at the camera with and without voltage applied, the rotation caused by the electric field can be determined.

The electro-optic crystal used was 0.5-mm-thick  $y$ -cut  $\text{LiTaO}_3$ , cut to completely cover the contact gap of the switch being studied. The top surface of the  $\text{LiTaO}_3$  was antireflection coated to prevent internal reflection and improve transmission through the crystal. The bottom surface was coated with the aforementioned dielectric mirror to have a reflectivity of 99.3% at 532 nm. The  $\text{LiTaO}_3$  optic axis ( $z$  axis) was perpendicular to the contact edges and generally parallel to the applied electric field. In this geometry, the crystal is sensitive primarily to the electric-field component parallel to the  $\text{LiTaO}_3$  optic axis. The voltage pulse switched by the green probe light was measured using an oscilloscope attached to the load side of the switch and was found to be negligible ( $10^{-6}$  times the applied bias voltage).

The complete probe system is shown in Fig. 42.25. The entire computer-controlled system consists of the test switch and crystal shown in detail in Figs. 42.23 and 42.24, the detector array, a high-voltage pulser, and an optical delay translation stage. The laser source is a Nd:YAG regenerative amplifier seeded by a Nd:YAG mode-locked oscillator. The wavelength is 1064 nm and the pulse width is about 100 ps to 200 ps. The mode-locked



Z768

Fig. 42.25  
The complete electro-optic imaging system.

pulses are amplified to approximately  $300 \mu\text{J}$  and switched out of the laser with a double Pockel's cell arrangement to yield pulses that have a prepulse to main pulse contrast ratio of 4000:1.<sup>9</sup> There are always small prepulses present in the amplifier output at the oscillator repetition rate of 100 MHz. The amplifier pulse repetition rate is variable up to 1 kHz. The infrared beam from the amplifier is first upcollimated and then split, 90% for switching use and 10% for second-harmonic generation. Green ( $\lambda = 532 \text{ nm}$ ) laser pulses are generated in a KTP crystal. This green beam is upcollimated and serves as the probe beam. The 1.25-cm, green-beam diameter is sufficient to completely illuminate all the electrode gaps that were studied. The back-reflected probe-beam pulses are imaged onto a  $512 \times 512$ -element GE CID camera, which is interfaced to a personal computer through a PCVISIONplus video frame grabber supplying an 8-bit digital image of the modulated probe beam. The camera response was measured to be linear with applied light intensity over the range used in this experiment. As the green probe consists of  $\sim 140$ -ps pulses, the switch surface field is sampled only during a short window in time. If the infrared excitation pulse illuminates the switch during this window, the switch field will be sampled during the photoconductive collapse. For surface switches, as in Fig. 42.24, this is

accomplished by directing an infrared pulse onto the switch gap collinear with the green probe pulse. For the bulk switches, the infrared illuminates the switch directly through the metallic mesh contacts. By sweeping the 140-ps sampling window in time, the switch surface field can be monitored as the switch photoconductivity evolves in time. The system's operation can be viewed as  $512 \times 512$  separate, parallel, pump-probe experiments, each probing a different spatial region in the electrode gap. The sampling window is moved in time by changing the length of an optical delay line in the infrared beamline. This delay line consists of a retro-reflector on an Aerotech computer-controlled translation stage. As the pump and probe are derived from the same laser pulse and timed optically, there is no jitter.

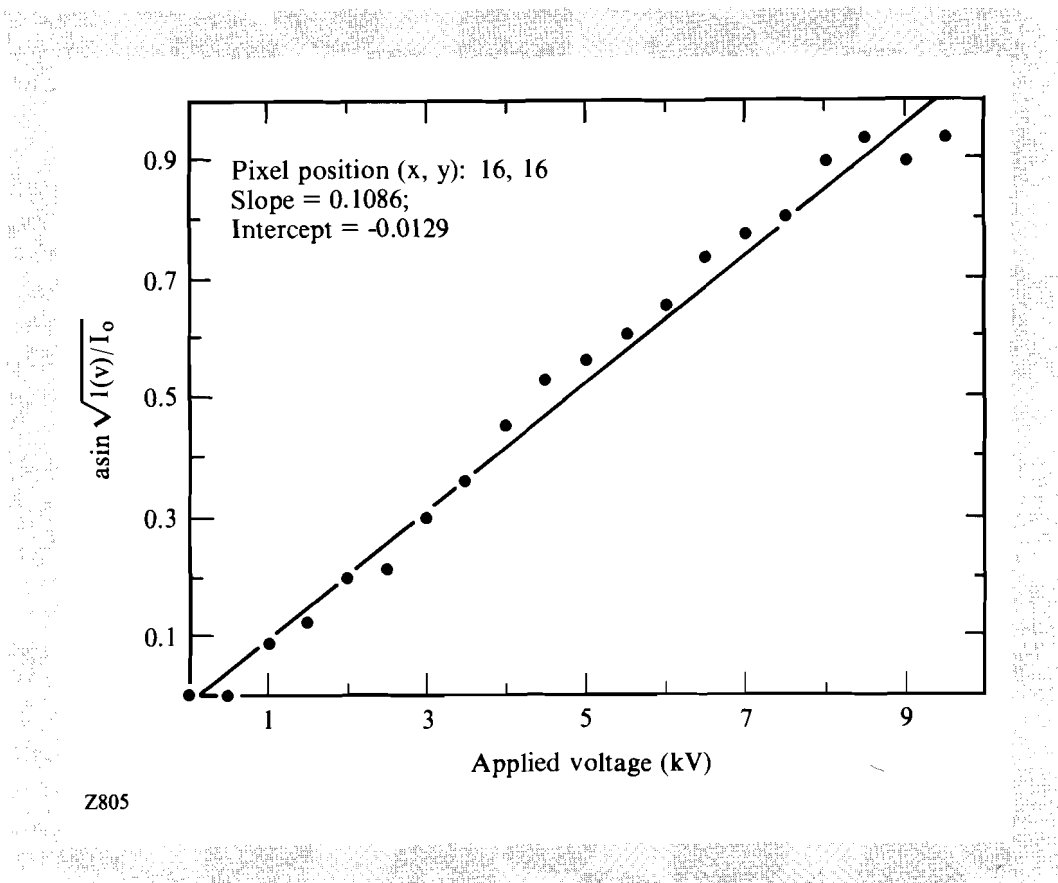
For the probe to operate in real time, i.e., without averaging, data must be collected with a single laser pulse. As the system operates in the high-field regime, the electric field applied to the electro-optic crystal causes the optical polarization vector of the probe pulse to change by a significant fraction of  $\pi/2$  ( $>2\%$ ). At these fields, the change in transmission to the camera is large with respect to the shot-to-shot noise in the laser pulse. Thus, the electro-optic images can be acquired without averaging. This is essential to image random events such as surface breakdown. To ensure that the camera sees only one laser pulse, the camera and laser are synchronized to the same electronic oscillator, with a pulse from the camera triggering the firing of the laser. Data is taken at a 30-Hz repetition rate, limited by the camera. The intensity of every laser pulse is measured with a fast diode. Any pulse not within 10% of a reference value is rejected and the measurement is repeated.

The field data must be extracted from the raw camera image. The values of  $\alpha_{i,j}$  and  $\beta_{i,j}$  for each point  $(i,j)$  must be determined so that given the transmission  $T_{i,j}$ , the field  $E_{i,j}$  can be determined. The crystal is not illuminated uniformly, as the probe beam has a Gaussian spatial profile. Therefore, the raw image must be normalized with respect to the beam profile, so that the transmissivity and not the transmitted intensity is used.

Each image acquired by the camera is normalized to a stored reference image. This reference image is the average of four frames taken with the quarter-wave plate set for maximum transmission and with a dielectric mirror in place of the  $\text{LiTaO}_3$  crystal. The light intensity is adjusted so that the most intense pixel is just within the 8-bit camera resolution; i.e., no points in the detector field are saturated. This reference image then contains  $I'_{i,j}$  for each point  $(i,j)$ , as in Eq. (1). Images normalized with respect to this reference are scaled to the maximum signal and represent  $I_{i,j}(V)/I'_{i,j}$ .

The values of  $\alpha_{i,j}$  and  $\beta_{i,j}$  are obtained by calibrating the response of the probe to an applied electric field. A quasi-dc, i.e., long compared to the light pulse, bias voltage is applied to the contacts by a computer-controlled high-voltage pulser. The bias voltage is varied from 0 kV–9.5 kV in 500-V increments. An image is taken at each voltage and reduced

to a  $32 \times 32$  array by averaging over pixels. This array size reduction is done so that image acquisition, processing, and display can be done with a PC rather than a workstation and in real time, i.e., without any post-processing. This allows for rapid scanning of camera images. The transmission curve [Eq. (1)] for each of the 1024 elements of the reduced image is determined experimentally by this procedure.  $\alpha_{i,j}$  and  $\beta_{i,j}$  are then obtained by performing a least-squares fit of the experimental transmission curve to Eq. (1) for each element in the reduced image. Figure 42.26 shows this dc calibration for one element of the reduced image. The biasing is chosen such that all points lie within one-half cycle of the transmission curve. Due to the sinusoidal nature of Eq. (1), it is sometimes necessary to reduce sensitivity to see large effects.



Z805

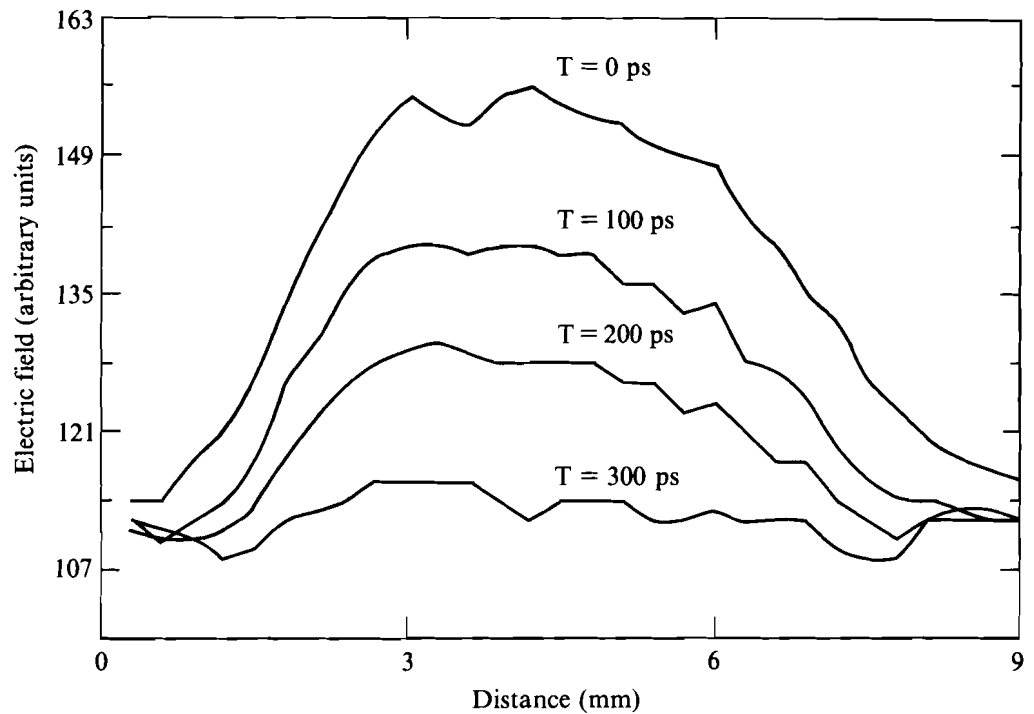
Fig. 42.26 Results of dc calibration of electro-optic imaging system showing least-squares fit of the experimental transmission curve to Eq. (1) for one image pixel.

After correcting for the probe-beam spatial profile and calibrating the crystal response, the surface electric field information can be decoded from the raw images. To measure the field, a frame is first acquired with high-voltage bias on and then with the bias off. Each frame is digitized with 8-bit resolution, normalized to the probe-beam profile and scaled, and then reduced to a  $32 \times 32$  array. The images are scaled by dividing the raw image by the reference image, pixel by pixel. The division is performed using a look-up table for speed of execution and scale control. These two reduced

arrays, i.e., each element within each array, represent two different points,  $T_{i,j}$ , on the transmission curve [Eq. (1)]. The zero-bias image is used to remove the contribution of the static birefringence. The arrays are used as inputs to a function that, using the dc calibration described earlier, transforms the transmission  $T_{i,j}$  to field  $E_{i,j}$  by inverting Eq. (1). The field  $E_{i,j}$  is given in units of “equivalent electrode voltage” (EEV), which means that the point  $(i,j)$  is responding to the applied electric field as if a voltage  $E_{i,j}$  were applied to the electrodes. The resulting field map of the electric field has an 8-bit range and can be displayed as a false-color image on a monitor or the digital image can be manipulated to produce field contour plots, axonometric plots, or field cross sections of a particular line across the switch. The optical system is capable of producing images with a spatial resolution of  $3\ \mu\text{m}$  per pixel. The electric field can be measured with this type of spatial resolution, but this would require that the above calibration procedure be applied to the entire  $512 \times 512$  array. This has been done in selected cases but, in general,  $32 \times 32$  images have been used. The minimum electric-field sensitivity is approximately  $200\ \text{V/cm}$  and can be adjusted by rotating the quarter-wave plate.

### Experiments

Silicon and GaAs photoconductive switches have been studied, the majority of the work involving GaAs. The Si switches are surface devices (see Fig. 42.23), whereas the GaAs switches are bulk devices (see Fig. 42.24). Figures 42.27 and 42.28 show typical raw, unnormalized data obtained with the electro-optic imaging system. Figure 42.27 shows successive lineouts of the surface field over a 3-mm-gap Si switch taken through the center of the switch parallel to the contact edge. The switch gap has been illuminated by the IR pump pulse. Time is relative to the position of the IR optical delay line, where 0 ps indicates the arrival of the pump pulse. The surface electric field begins collapsing at the onset of photoconductive switching and has collapsed completely within 300 ps, consistent with the  $\sim 200$ -ps pulse width of the laser. Figure 42.27 illustrates the ability of the system to monitor the surface field in the switch gap during switch operation and the ability to measure switching parameters like switch rise time directly using the field across the electrode gap and not by measuring the switched output. In this case, the field collapse is spatially uniform, as the gap was driven conductive by uniform IR illumination. Figure 42.28 illustrates the ability of the system to map nonuniform fields above a 3-mm-gap Si switch and to observe carrier migration within the switch gap. The nonuniform fields are the result of nonuniform IR illumination. The center of the switch gap was illuminated with a pinpoint ( $\sim 40\text{-}\mu\text{m}$ ) spot of infrared laser energy. This local illumination photogenerates carriers only in a small region at the gap center. These carriers migrate outward, collapsing the surface field as they drift. One interesting feature of the field on the coplanar silicon switch is that we have not detected the significant field enhancements at the contact edge we would have suspected from the geometry. We believe that this may be because of the conductivity of the silicon substrate.



Silicon substrate, 3-mm contact gap. 5.8-kV bias

Z770

Fig. 42.27

Collapse of electric field above IR-illuminated surface-type Si switch. Lineouts from raw electro-optic images taken through center of switch perpendicular to contact edge for various times. The switch was biased at 5.8 kV across a 3-mm contact gap. Note the spatially uniform collapse of the field.

The primary physical system investigated was the collapse of the electric field in a GaAs bulk photoconductive switch. These switches were fabricated by depositing circular contacts of NiAu:Ge on opposite faces of a 0.6- to 1-cm-thick block of intrinsic GaAs. The GaAs was high-resistivity material ( $\rho \sim 10^7$  cm) supplied by MA-COM. The contacts consisted of a solid annulus surrounding a center region that was perforated to allow light to pass through into the bulk of the GaAs. The contact preparation was also varied with the 6-mm-thick switches having an ion implantation under the metallization to make ohmic contacts, the other samples having contacts deposited on bare GaAs. This switch design is of particular interest both for its applicability to coaxial geometry<sup>10</sup> and for its relative immunity to surface breakdown, as a surface arc must travel out to the edge, down the side, and back into the center—a very long physical path. The design is also useful in that this contact geometry allows for uniform fields that facilitate extraction of absolute field values, as opposed to the coplanar geometry that

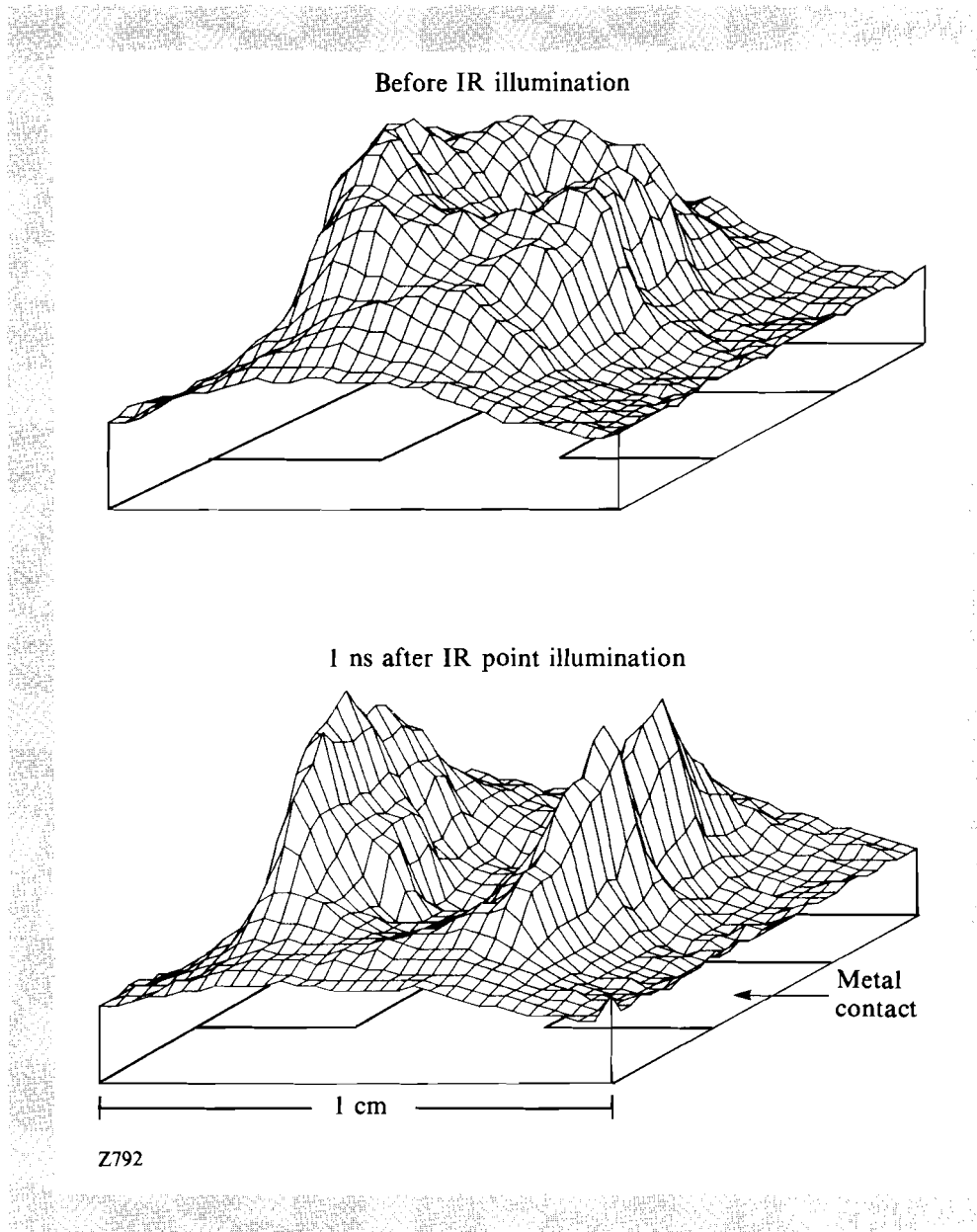
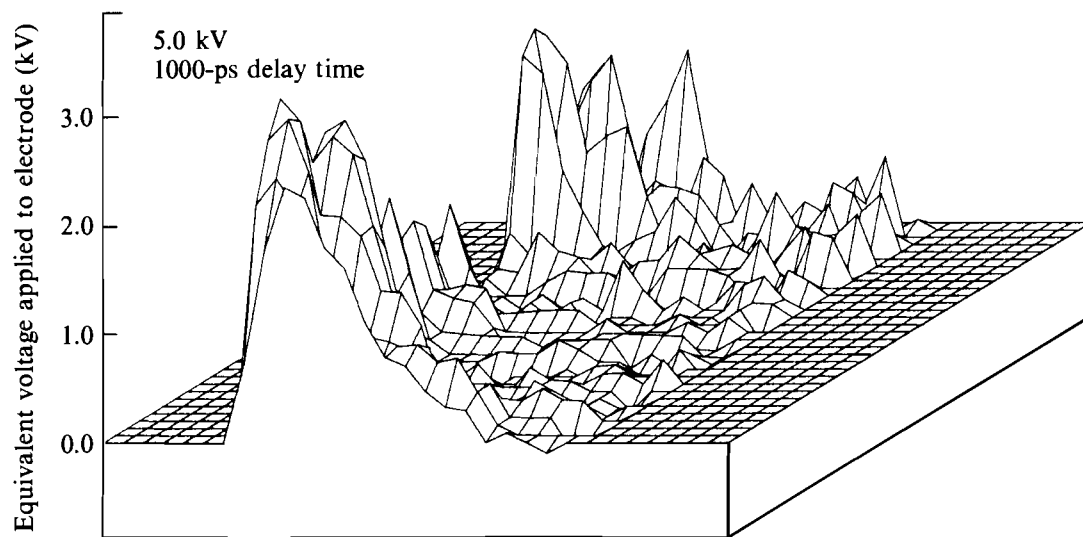


Fig. 42.28  
 Effect of nonuniform illumination on the electric field above Si surface-type switch. Raw electro-optic images shown before and 1 ns after illumination by 40-mm spot of IR energy at switch center. Switch was biased at 3 kV across 3-mm contact gap. Note local collapse of electric field near switch center.

has a much more complicated field pattern. To access the fields between the contacts, this design has been modified by cutting the GaAs in a plane passing through the center of the contacts. Connection to the external circuit was made by pressure-contacting copper electrodes coated with indium along the outside circumference of the NiAu:Ge electrodes. The Cu electrodes were bored out so that IR light could reach the switch contacts. By

placing a dielectric beam splitter in the IR pump beam, approximately 50% of the IR light could be directed onto each electrode. Either of these beams could be blocked to investigate asymmetries in the response of the photoconductor. The arrival time of the two beams at the switch was adjusted to within 300 ps by monitoring the arrival of the switch pulse at the load with a 1-GHz analog oscilloscope. The dielectric beam splitter was mounted on a kinematic mount so that it could be removed and the full IR laser energy could be applied to one side of the switch. Thus, five illumination schemes were employed, considering that full energy could be applied to either the ground or high-voltage contact.

Figures 42.29–42.32 show data taken for a 6-mm-thick ion-implanted GaAs bulk switch. The images taken were normalized and scaled to EEV. Figure 42.29 shows an axonometric plot of the surface field on a 6-mm GaAs switch illuminated through both contacts 800 ps after initial illumination by a 2-mm-wide pump beam. Outside the region between the contacts, the field falls abruptly to zero because there is no tangential component of the electric field at the surface of a conductor. Noise spikes in that region of the image have been artificially suppressed. The left edge of the image corresponds to the negative high-voltage contact, and the right side to the ground contact.



Z809

Fig. 42.29

The electro-optic image of the surface electric field on a GaAs switch 800 ps after illumination by a 200-ps IR pulse through both of its electrodes. The left side of the image corresponds to negative high-voltage electrode. The active area is 6 mm by 10 mm and the field enhancements are located behind the solid portion of the high-voltage contact.

The active area in the center is 6 mm wide, and the front and back edges of the image are 10 mm apart and correspond to the edges of the deposited electrodes. Initially, the image was uniform between the contacts. The infrared light has caused the field to collapse. The center section of the image is where the 2-mm-wide pump beam illuminated the GaAs. Note that the field has collapsed over most of the active region to a value of  $\sim 0.3$ -kV EEV although the bias voltage is 5 kV. The field collapses uniformly on the ground side of the image but it has areas of significant enhancement on the high-voltage side. There are two significant high-voltage spikes of  $\sim 3$ -kV EEV even though most of the switch field has collapsed. These spikes are located at the very edges of the high-voltage contact (review Fig. 42.24 for contact geometry). A survey of all the acquired images reveals that this is a general feature independent of the type of contact. There is always an enhancement at the high-voltage contact. The enhancement can be alleviated at the perforated region of the contact by illuminating with more IR light but the collapse is never as complete as on the ground side.

Figures 42.30 and 42.31 show a series of axonometric plots of the field above a 6-mm GaAs switch. These illustrate the progressive collapse of the

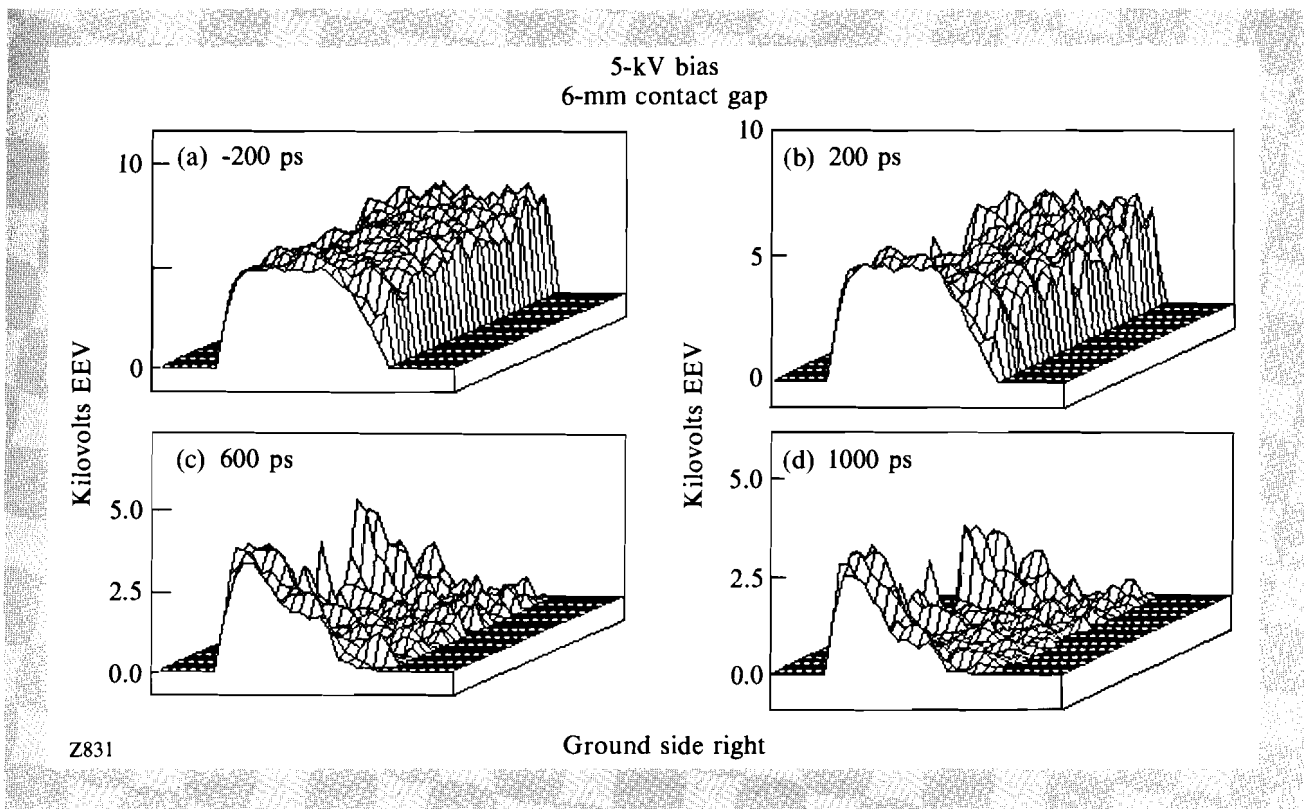
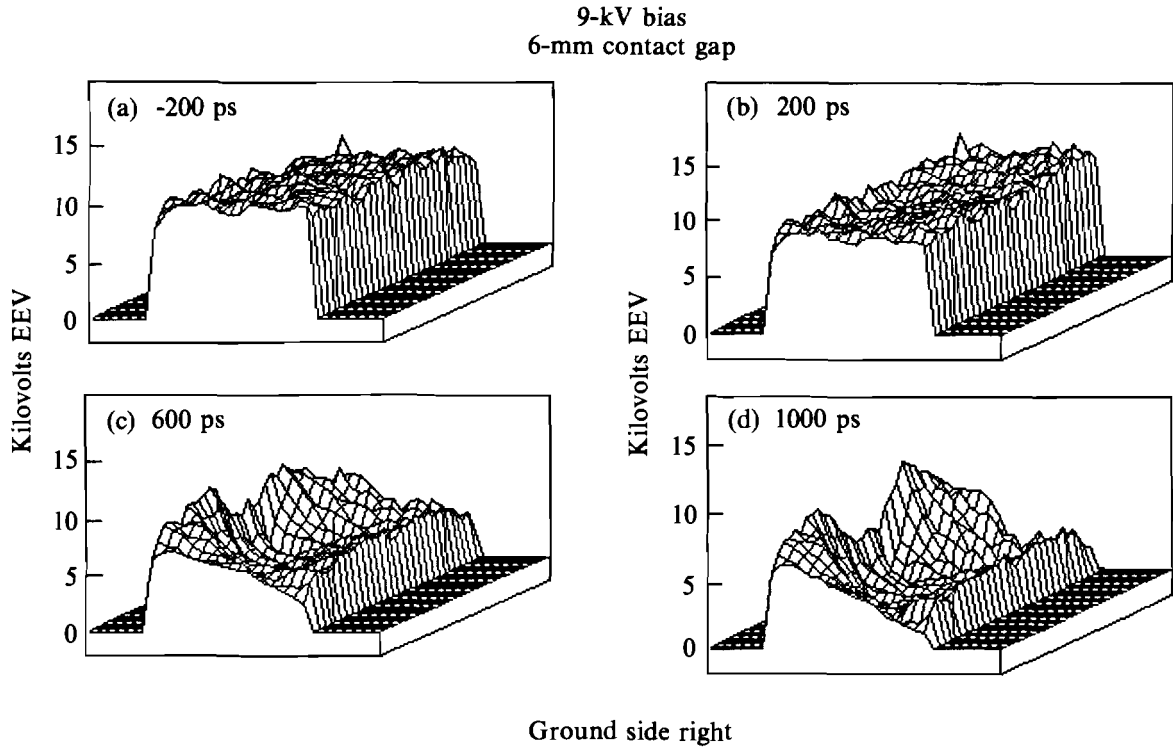


Fig. 42.30 Temporal evolution of electric field above 6-mm-thick bulk GaAs switch illuminated by 200-ps IR pulse through both contacts. Switch biased at 5 kV. Images processed and scaled to equivalent electrode voltage (EEV). The active area of the image is 6 mm by 1 cm. The collapse of electro-optic field proceeds from the essentially uniform profile shown in (a).

surface field in time for two different bias voltages. Both contacts were illuminated with IR light. In Fig. 42.30, the switch bias was 5 kV; in Fig. 42.31, 9 kV. The field is given in EEV, the true field is EEV divided by the gap distance—in this case, 6 mm. The time is relative to the IR translation-stage position; 0 ps is the arrival of the IR pulse and the stage can scan out to 1 ns after IR illumination begins. At -200 ps, the field across the switch is essentially uniform, as expected; as time progresses, the field collapses. For 5-kV bias, the collapse is almost complete, except for the enhancement

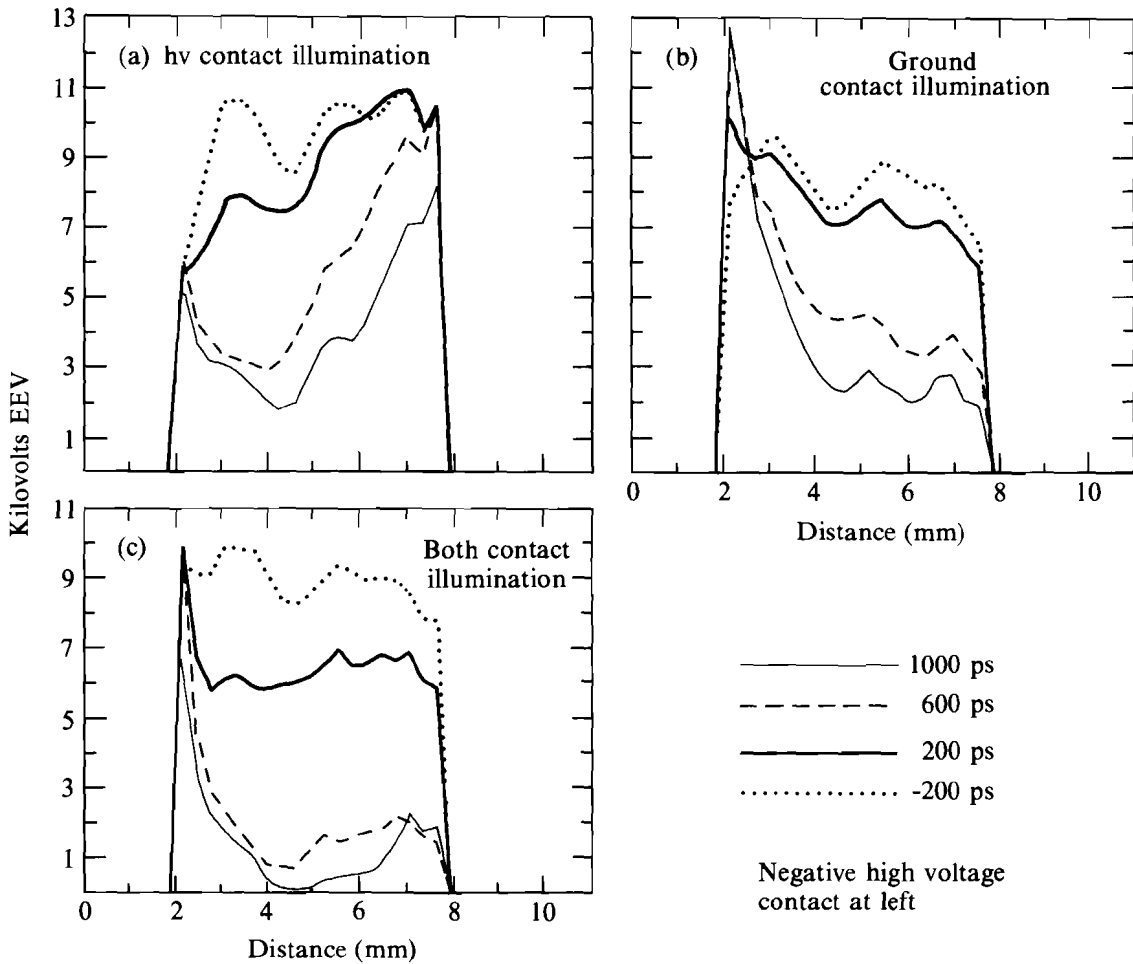


Z830

Fig. 42.31  
Same conditions as in Fig. 42.30 except switch biased at 9 kV. The incomplete collapse of field is evidenced by ~3 kV/cm field remaining across switch after 1200 ps.

near the contacts. At 9 kV, the situation is much different: the field collapses only to 3-kV EEV. There is still a field of ~3 kV/cm across the switch, 1 ns after illumination.

Figure 42.32 shows a series of lineouts from surface-field images of the 6-mm GaAs switch, taken through the center of the image, perpendicular to the contact faces. These illustrate the progressive collapse of the surface field in time for various illumination schemes. Switch bias was 8 kV.



Z834

Fig. 42.32

Temporal evolution of electric field above 6-mm-thick bulk GaAs switch for different illumination conditions. Switch biased at 8 kV. Lineouts taken through center of processed electro-optic image at different times after illumination with 200-ps IR pulse. Greater efficiency and speed are obtained for illumination through both contacts.

Single-sided illumination is characterized by a wave front that propagates across the switch. In Figs. 42.32(a) and 42.32(b), the field collapses from the illuminated contact to the nonilluminated contact in time as the region of conduction propagates from the region of photogeneration. When both sides are illuminated [Fig. 42.32(c)], the field collapses more quickly and to a lower final value than for single-sided illumination, as in Figs. 42.32(a) and 42.32(b). Switch rise time is faster and the efficiency is higher for illumination through both contacts—an important engineering consideration. The field enhancement exhibited in Figs. 42.29–42.31 can also be observed in these lineouts. Small differences in the -200-ps lineouts may be caused

by the small prepulses that excite the switch before the main IR pulse arrives, as well as the laser-intensity fluctuation ( $\sim 10\%$ ).

Some of these observations can be made more quantitative by defining an electro-optic switching efficiency. A standard measure of switching efficiency would be the fraction of the dc bias that is switched to the load. A perfectly efficient switch would be driven completely conductive and the bias voltage would appear across the load. No electric field would remain across the switch electrodes. If the electric field across the switch is imaged electro-optically, an electro-optic switching efficiency  $\eta$  can be defined:

$$\eta = \sum_N \eta_{i,j} = (1/N) \sum_N [E'_{i,j} - E_{i,j}(t) / E'_{i,j}], \quad (2)$$

where the summation is over the total number of active pixels (pixels outside the electrode gap have been ignored),  $E'_{i,j}$  is the electro-optic image element with no IR light present, and  $E_{i,j}(t)$  is the electro-optic image element at a time delay  $t$  as determined by Eq. (1). The restrictions on the summation are that if

$$E'_{i,j} - E_{i,j}(t) < 0, \quad (3)$$

corresponding to a field enhancement  $\eta$ , was set equal to zero (i.e., it was considered to be an element that had not undergone switching) and if

$$E'_{i,j} - E_{i,j}(t) > E'_{i,j}, \quad (4)$$

implying a negative oscillation in the surface electric field, the efficiency at that point  $\eta$  was set equal to 1. The parameter  $\eta$  is a measure of how much of the dc surface field has been switched, and would measure the total field switched if it were possible to integrate through the entire switch volume. Although this is impossible for these experiments,  $\eta$  still gives a good indication of switch efficiency. Figure 42.33 shows the electro-optic efficiency as a function of the optical delay-line setting for several applied fields in the case of two-sided illumination. The most striking feature of this graph is that the switching efficiency drops as the field increases. Figure 42.34 shows that this trend continues with single-sided illumination at two different intensities. For example, at an illumination intensity of  $2.1 \text{ mJ/cm}^2$ , there is sufficient light to switch a field of  $6.6 \text{ kV/cm}$  with 90% efficiency. At the same intensity, a field of  $15 \text{ kV/cm}$  is switched with only 40% efficiency. Figure 42.34(a) shows that increasing the intensity to  $3.8 \text{ mJ/cm}^2$  increases the efficiency to only 50% at  $15 \text{ kV/cm}$ . The rise time of the switch also decreases as the light intensity is increased.

### Discussion

A number of important features regarding the operation of GaAs photoconductive switches can be discerned from this work. First, the electric

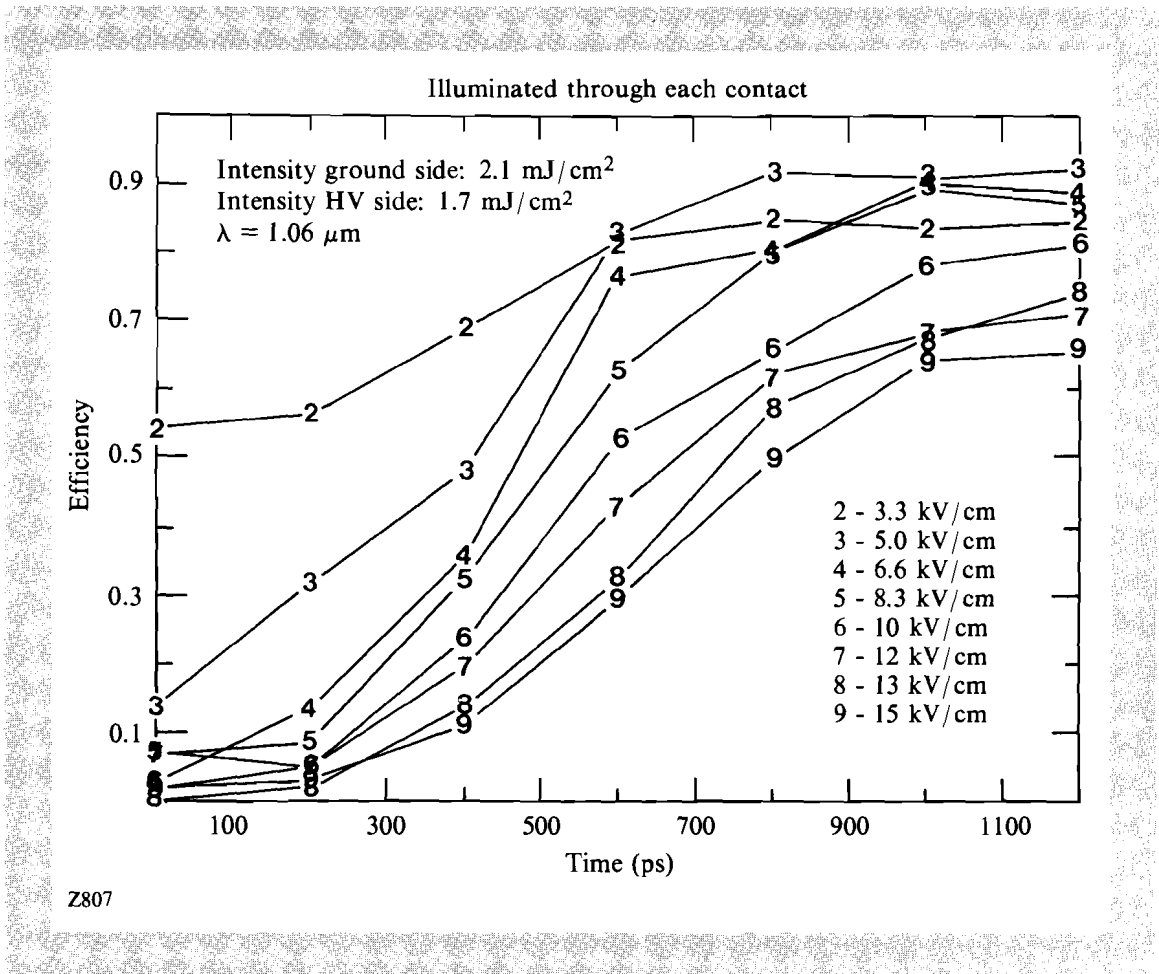
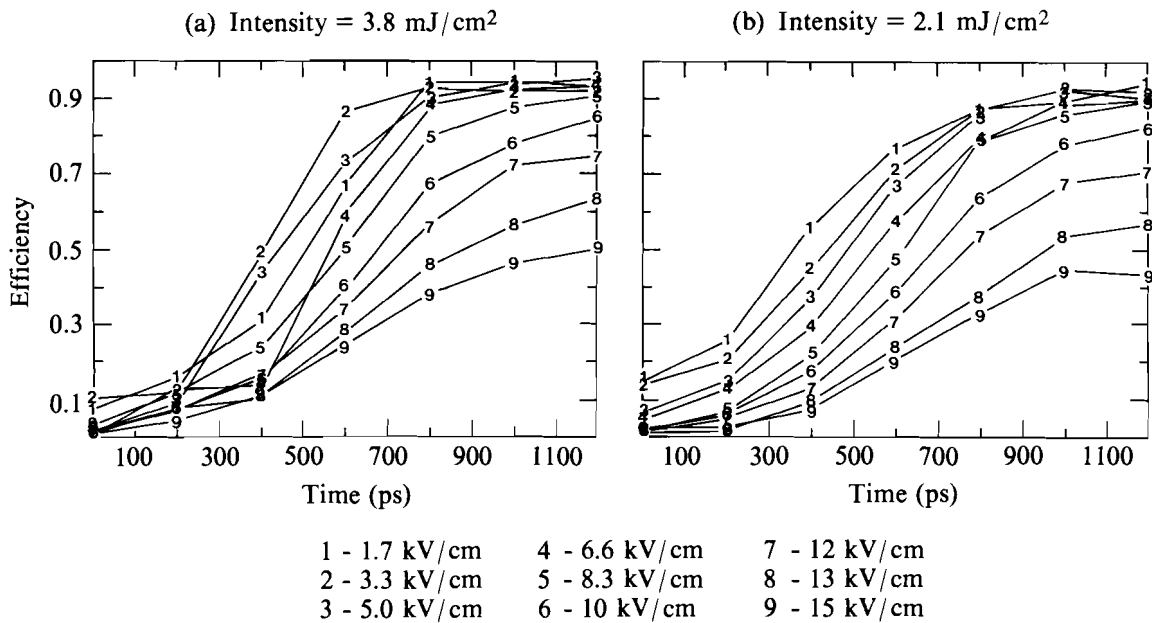


Fig. 42.33  
 The electro-optic efficiency for a 6-mm bulk GaAs photoconductive switch illuminated through both contacts as a function of time. The efficiency decreases with increasing field.

field is enhanced at the negative high-voltage electrode and collapses most slowly there. This type of behavior was seen in both types of contacts tested. Similar behavior has been predicted to occur at both contacts for uniformly illuminated silicon switches with ohmic contacts.<sup>11</sup> The field enhancement, in that case, was shown to be caused by rapid carrier sweep-out at the ohmic contacts. It is possible that ohmic contacts at the negative electrode are responsible for the field enhancement observed in the data. In particular, the enhancement was strongest under the solid portion of the high-voltage contact. A corresponding enhancement was not observed on the ground-side electrode (positive with respect to the high-voltage pulse). This enhancement was reduced in the perforated region by increasing the light incident on the high-voltage contact. This enhancement was seen in all samples and showed some increase with the number of shots applied to the sample. Thus, some of the nonuniform enhancement may have been associated with the long-term degradation of the contact ( $>2 \times 10^4$  shots) due to arcing from the perforated region to the solid region of the NiAu:Ge contact. This arcing only occurred if the GaAs was switched.



Z806

Fig. 42.34

The electro-optic efficiency of a GaAs photoconductive switch illuminated through only the high-voltage contact; (a) 3.8 mJ/cm<sup>2</sup>, (b) 2.1 mJ/cm<sup>2</sup>.

The switching efficiency of GaAs decreased with increasing voltage. Increasing the number of carriers by increasing the IR illumination energy by a factor of ~2 does not significantly improve switching efficiency, suggesting that switching efficiency is predominantly a field effect. This is confirmed by the observation that, for constant bias voltage, the switching efficiency increases with increasing electrode spacing, although this data is not presented here. The measured decrease in switching efficiency with increasing voltage may well be caused by the negative differential resistance in GaAs.<sup>12</sup> Above 3 kV/cm, the electron drift velocity in GaAs decreases as the electric field increases. Since the current is proportional to the drift velocity, this represents an effective increase in switch resistance as the field increases above 3 kV/cm. This observation has important implications for the use of photoconductive switches in pulsed-power applications. In many cases, the trend has been to push the breakdown limit in these devices to achieve the highest switch electrical energy for the minimum optical energy. These results indicate that switches with larger gaps and lower bias fields are much more efficient in terms of switched voltage for a given pump energy.

The electrode geometry of the Si surface switches results in a very nonuniform field between the contacts, making calibration and extraction of

absolute field values difficult. Also, Si switch surface fields were greatly affected by the aforementioned laser prepulses, again making field measurements difficult. However, the lack of significant peaking at the contacts and the different modes of collapse with different illuminator regimes show some of the underlying carrier dynamics.

The two-dimensional electro-optic imaging system can time resolve the full spatial and temporal variations of the electric field on semiconductor surfaces. The images have provided significant insight into the mechanism of photoconductive switching in GaAs. The primary strength of this diagnostic is its ability to monitor events inside the electrode gap itself, which is a distinct advantage over monitoring only the semiconductor device output waveform. Switching parameters can be measured with no electrical connection to the high-voltage circuit. Extension of this work to integrated circuits could allow the characterization of devices without introducing connector or strip-line effects. Future work will center around using the electro-optic imaging system to investigate the phenomena of surface breakdown and further the study of semiconductor photoconductivity. Images obtained with the system should provide an appropriate experimental basis for a complete model of the photoconductive process.

#### ACKNOWLEDGMENT

This work was supported by the Laser Fusion Feasibility Project at the Laboratory for Laser Energetics, which has the following sponsors: Empire State Electric Energy Research Corporation, New York State Energy Research and Development Authority, Ontario Hydro, and the University of Rochester, and also by the SDIO/IST and managed by the Office of Naval Research under contract N00014-86-K-0583. Such support does not imply endorsement of the content by any of the above parties.

The GaAs was supplied by M. Weiner, A. Kim, and R. Zeto at the U.S. Army Electronics Technology and Device Laboratory.

#### REFERENCES

1. G. Mourou, W. H. Knox, and S. Williamson, *Picosecond Optoelectronic Devices*, Chap. 7 (Academic Press, New York, NY, 1984), p. 219.
2. C. Bamber, W. Donaldson, T. Juhasz, L. Kingsley, and A. C. Melissinos, *Part. Accel.* **23**, 255 (1988).
3. J. A. Valdmanis, G. Mourou, and C. W. Gabel, *Appl. Phys. Lett.* **41**, 211 (1982).
4. K. Meyer, M. Pessot, G. Mourou, R. Grondin, and S. Chamoun, *Appl. Phys. Lett.* **53**, 2254 (1988).
5. LLE Review **34**, 74 (1988).
6. Z. H. Zhu, J.-P. Weber, S. Y. Wang, and S. Wang, *Appl. Phys. Lett.* **49**, 432 (1986).
7. Y. H. Lo *et al.*, *Appl. Phys. Lett.* **50**, 1125 (1987).
8. A. Yariv, *Quantum Electronics*, 2nd ed., Chap. 14 (John Wiley & Sons, New York, NY, 1975), p. 327.
9. I. N. Duling III, T. Norris, T. Sizer II, P. Bado, and G. A. Mourou, *J. Opt. Soc. Am. B* **2**, 616 (1985).

10. L. Bovino *et al.*, *Digest of Technical Papers*, 5th IEEE Pulse Power Conference, edited by P. Turchi and M. F. Rose (IEEE, New York, NY, 1985), p. 242.
11. A. E. Iverson, *Trans. Soc. Comput. Simulation* **5**, 175 (1988).
12. S. M. Sze, *Physics of Semiconductor Devices* (John Wiley & Sons, New York, NY, 1981), p. 44.